The Role of Homolytic Bond Dissociation Energy in the Deprotonation of Cation Radicals. Examples in the NADH Analogues Series

Agnès Anne, Sylvie Fraoua, Valérie Grass, Jacques Moiroux,* and Jean-Michel Savéant*

Contribution from the Laboratoire d'Electrochimie Moléculaire de l'Université Denis Diderot, Unité Associée au CNRS No 438, 2 place Jussieu, 75251 Paris Cedex 05, France

Received October 27, 1997

Abstract: The deprotonation of the cation radical of 9-cyanomethylacridane by a series of normal bases is investigated and its pK_a and homolytic bond dissociation energy determined experimentally. The latter parameter has the largest value in the NADH analogue series, thanks to the strong destabilization of the corresponding cation by the cyano group. It thus allows a significant extension of the attempted correlation between the intrinsic barriers and homolytic bond dissociation energies (D). Aside from members of the series where bulky substituents cause a decelerating steric effect, the correlation is close to a proportionality to D/4. The same correlation applies for all the other cation radicals where the rate constants of deprotonation by normal bases are available. The respective contributions of the homolytic and ionic states in the dissociation of the two types of acid, cation radicals and the conjugate acid of the normal base, are such that a simple model can be developed which regards the deprotonation reaction as a concerted H atom/one-electron transfer. It explains why, for each cation radical, the deprotonation by normal bases gives rise to a single Brönsted plot and why the intrinsic barriers are proportional to D/4. In the NADH analogue series, the deviations from proportionality observed with bulky substituents, and to a lesser extent, upon changing the extent of charge delocalization over the cation radical molecule are accounted for by product and reactant work terms, respectively.

Deprotonation of hydrocarbons requires some form of activation of the carbon atom for the reaction to be amenable to thermodynamic and kinetic characterization. There are two main ways for decreasing the pK_a of carbon−hydrogen bonds. One involves the decrease of the electron density on the carbon atom by means of an electron withdrawing group directly borne by the carbon or located in a conjugated position to it on an unsaturated substituent.[1−3] The other consists of oxidizing the substrate so as to produce the corresponding cation radical. The resulting decrease in electron density induces a considerable decrease in the pK_a as compared to the parent molecule.[4,5] The kinetics of the deprotonation of several families of cation radicals have been measured.[6−14] Among them the NADH analogues series offers two advantageous features.[14] One is that the cation obtained after deprotonation of the cation radical and further electron abstraction (Scheme 1) is stable. The rates of deprotonation can thus be unambiguously determined in the framework of the mechanism depicted in Scheme 1. Combining the use of direct electrochemistry, redox catalysis, and laser flash photolysis, they could be determined up to the diffusion limit,

Scheme 1

$$AH - e^- \rightleftharpoons AH^{\bullet+}$$
$$AH^{\bullet+} + B \rightleftharpoons A^\bullet + BH^+$$
$$A^\bullet - e^- \longrightarrow A^+$$
$$A^\bullet + AH^{\bullet+} \longrightarrow A^+ + AH$$

(1) (a) Bell, R. P.; Goodall, D. M. *Proc. R. Soc. London, Ser. A* **1966**, *294*, 273. (b) Bordwell, F. G.; Boyle, W. J. *J. Am. Chem. Soc*. **1972**, *94*, 3907. (c) Albery, W. J.; Campbell-Crawford, A. N.; Curran, J. S. *J. Chem. Soc., Perkin Trans.* **1972**, 2206.

(2) (a) Bernasconi, C. F. *Tetrahedron* **1985**, *41*, 3219. (b) Bernasconi, C. F. *Acc. Chem. Res.* **1987**, *20*, 301. (c) Bernasconi, C. F. *Adv. Phys. Org. Chem.* **1992**, *27*, 119.

(3) Terrier, F.; Boubaker, T.; Xiao, L.; Farrell, P. G. *J. Org. Chem.* **1992**, *57*, 3924. (b) Moutiers, G.; El Fahid, B.; Goumont, R.; Chatrousse, A. P.; Terrier, F. *J. Org. Chem.* **1996**, *61*, 1978.

(4) (a) Nicholas, A.; Arnold, D. R. *Can. J. Chem*. **1982**, *60*, 2165. (b) Nicholas, A.; Boyd, R. J.; Arnold, D. R. *Can. J. Chem*. **1982**, *60*, 3011.

(5) (a) Bordwell, F. G.; Cheng, J. P. *J. Am. Chem. Soc*. **1989**, *111*, 1792. (b) Zhang, X.; Bordwell, F. G. *J. Org. Chem.* **1992**, *57*, 4163. (c) Zhang, X.; Bordwell, F. G.; Bares, J. E.; Cheng, J. P. *J. Org. Chem.* **1993**, *58*, 3051.

(6) (a) Schlesener, C. J.; Amatore, C.; Kochi, J. K. *J. Am. Chem. Soc.* **1984**, *106*, 7472. (b) Schlesener, C. J.; Amatore, C.; Kochi, J. K. *J. Phys. Chem.* **1986**, *90*, 3747. (c) Masnovi, J. M.; Sankararaman, S.; Kochi, J. K. *J. Am. Chem. Soc.* **1989**, *111*, 2263. (d) Sankararaman, S.; Perrier, S.; Kochi, J. K. *J. Am. Chem. Soc.* **1989**, *111*, 6448.

(7) (a) Bacciochi, E.; Del Giacco, T.; Elisei, F. *J. Am. Chem. Soc.* **1993**, *115*, 12290. (b) Bacciochi, E.; Bietti, M.; Putignani, L.; Steenken, S. *J. Am. Chem. Soc.* **1996**, *118*, 5952.

(8) (a) Dinnocenzo, J. P.; Banach, T. E. *J. Am. Chem. Soc*. **1989**, *111*, 8646. (b) Dinnocenzo, J. P.; Karki, S. B.; Jones, J. P. *J. Am. Chem. Soc.* **1993**, *115*, 7111.

(9) (a) Xu, W.; Mariano, P. S. *J. Am. Chem. Soc*. **1991**, *113*, 1431. (b) Xu, W.; Zhang, X. ; Mariano, P. S. *J. Am. Chem. Soc.* **1991**, *113*, 8863.

(10) (a) Reitstöen, B.; Parker, V. D. *J. Am. Chem. Soc.* **1990**, *112*, 4698. (b) Parker, V. D.; Chao, Y.; Reitstöen, B. *J. Am. Chem. Soc.* **1991**, *113*, 2336. (c) Parker, V. D.; Tilset, M. *J. Am. Chem. Soc.* **1991**, *113*, 8778.

(11) (a) Fukuzumi, S.; Kondo, Y.; Tanaka, T. *J. Chem. Soc., Perkin Trans. 2* **1984**, 673. (b) Fukuzumi, S.; Tokuda, Y.; Kitano, T.; Okamoto, T.; Otera, J. *J. Am. Chem. Soc.* **1993**, *115*, 8960.

(12) Sinha, A.; Bruice, T. C. *J. Am. Chem. Soc.* **1984**, *106*, 7291.

(13) (a) Tolbert, L. M.; Khanna, R. K. *J. Am. Chem. Soc.* **1987**, *109*, 3477. (b) Tolbert, L. M.; Khanna, R. K.; Popp, A. E.; Gelbaum, L.; Bettomley, L. A. *J. Am. Chem. Soc.* **1990**, *112*, 2373.

(14) (a) Hapiot, P. ; Moiroux, J.; Savéant, J.-M. *J. Am. Chem. Soc.* **1990**, *112*, 1337. (b) Anne, A.; Hapiot, P.; Moiroux, J.; Neta, P.; Savéant, J.-M. *J. Phys. Chem.* **1991**, *95*, 2370. (c) Anne, A.; Hapiot, P.; Moiroux, J.; Neta, P.; Savéant, J.-M. *J. Am. Chem. Soc.* **1992**, *114*, 4694. (d) Anne, A.; Fraoua, S.; Hapiot, P.; Moiroux, J.; Savéant, J.-M. *J. Am. Chem. Soc.* **1995**, *117*, 7412.

S0002-7863(97)03725-6 CCC: $15.00
Published on Web 03/13/1998

Scheme 2

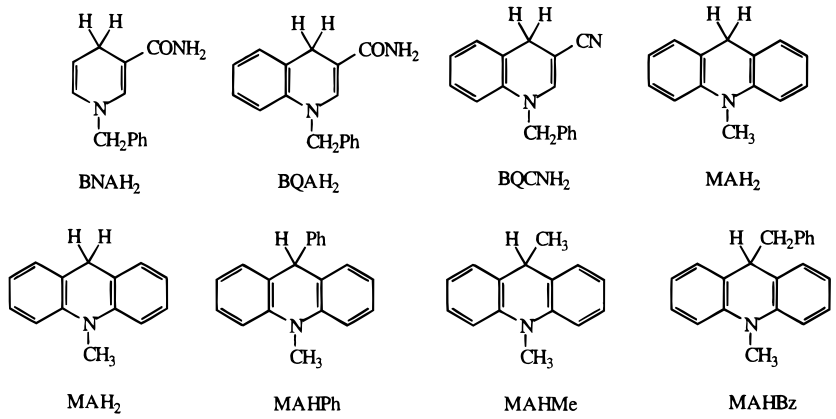

thus allowing the construction of extended Brönsted plots, which is rarely the case for other cation radicals. Another advantage of this series of cation radicals is that key thermodynamic parameters, such as their pK_a's and homolytic bond dissociation energies, can be derived from experimentally measurable quantities through appropriate thermodynamic cycles.

Knowing the pK_a's, extrapolating the Brönsted plots to $\Delta pK_a = 0$ has allowed the determination of the intrinsic barrier free energies, i.e., the activation free energy for $\Delta G^0 = (RT/F)\Delta pK_a = 0$, $\Delta G^{\ddagger}_{\Delta G^0=0}$, of a series of NADH analogues cation radicals. It was observed that a correlation exists between $\Delta G^{\ddagger}_{\Delta G^0=0}$ and the homolytic bond dissociation energy, D, ($AH^{\bullet+} \leftrightarrow A^+ + H^{\bullet}$) suggesting that proton abstraction from these cation radicals may be viewed as a concerted H-atom/electron transfer rather than a *stricto sensu* proton transfer.[14]

In order to further test the validity of that correlation we have attempted to enlarge the range of variation of the cation radical bond dissociation energy by introducing electron-withdrawing or electron-donating substituents on the carbon bearing the dissociating hydrogen. The cyano derivative appears to be a good candidate to obtain a maximal value of D, since the cyano group is expected to strongly destabilize the cation resulting from the homolytic cleavage of the carbon−hydrogen bond. This is indeed what we have found with the cation radical of the 9-cyano derivative of *N*-methylacridane, MAHCN. The determination of the deprotonation rate constant by a series of bases and of the pertinent thermodynamic parameters is described in the next section. We have also investigated the 9-methoxy derivative. However, its deprotonation cannot be observed in the accessible range of pH's. Rather, it cleaves off the methoxy group as well as the methyl group borne by the nitrogen. These reactions will be described elsewhere.

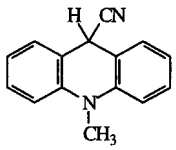

MAHCN

The second part of the paper is devoted to modeling the dynamics of cation radical deprotonation based on the main experimental characteristics of the reaction, namely, (i) the fact that a single Brönsted plot is obtained when a cation radical is opposed to a series of "normal" nitrogen or oxygen bases, (ii) the fact that the intrinsic barrier is relatively large, large enough for the deprotonation reaction to be under activation control in most of the accessible pH range, and (iii) the observation that the intrinsic barrier free energy correlates with the bond dissociation energy. For the reasons given above, the NADH analogues series will serve as the main experimental example for a quantitative discussion. The results obtained with other cations radical cations will also be discussed insofar sufficient kinetic and thermodynamic data are available.

Concerning point (iii), it is found, in the NADH analogues series, that $\Delta G^{\ddagger}_{\Delta G^0=0}$ varies approximately as $D/4$. However small deviations from this relationship appear as a function of the nature of the rings in the AH series depicted in Scheme 2. More important deviations are observed in the MAHR (R = Ph, Me, Bz) series (Scheme 2) pointing to the existence of some sort of steric effect. These two effects will be discussed in the framework of the proposed model.

Table 1. Thermodynamic Data[a]

compound	MAHCN	MAH_2[b]
$E^0_{AH/AH^{\bullet+}}$	0.985 ± 0.005	0.860 ± 0.004
$E^0_{A^{\bullet}/A^+}$	0.010 ± 0.002	−0.465 ± 0.010
$E^0_{AH/A^+,pH=0}$	0.370 ± 0.028 (±0.008)[c]	0.220 ± 0.024 (±0.004)[c]
$pK_{a\ AH^{\bullet+}}$	−4.4 ± 1.1 (±0.4)[c]	0.8 ± 1.1 (± 0.3)[c]
D[d] (eV)	2.115 ± 0.066 (±0.026)[c]	1.800 ± 0.070 (±0.030)[c]
$D_{AH/A^{\bullet}+H^{\bullet}}$[e]	3.09 ± 0.066 (±0.026)[c]	3.125 ± 0.070 (±0.030)[c]

[a] In acetonitrile. All potentials are referred to the aqueous saturated KCl saturated calomel electrode. [b] From ref 14c. [c] The main part of the uncertainty (±0.020 V on $E^0_{MAHZ/MAZ^+,pH=0}$, ± 0.7 on $pK_{a\ MAHZ^{\bullet+}}$, ± 0.041 eV on D originates from the uncertainty on $E^0_{NQH_2/NQ,pH=0}$ (see text and refs 14a,c). The numbers between parentheses represent the uncertainty for one NADH analogue relative to the others. [d] Bond dissociation energy of the cation radical. [e] Bond dissociation energy of the parent substrate.

Results

MAHCN was prepared by the reaction of MAH^+ with CN^- ions as depicted in the Experimental Section. The thermodynamic and kinetic parameters were determined as follows.

Thermodynamic Characteristics. The data obtained for MAHCN, following the procedures depicted below are summarized and compared with the values obtained for MAH_2 in Table 1.

The determination of the $pK_{a\ AH^{\bullet+}}$'s requires the determination of two one-electron standard potentials, $E^0_{AH/AH^{\bullet+}}$ and $E^0_{A^{\bullet}/A^+}$, and of a two-electron standard potential, $E^0_{AH/A^+,pH=0}$, corresponding to the hydride transfer reaction

$$AH \rightleftharpoons A^+ + 2e^- + H^+ (H^-)$$

taken at pH = 0:

$$pK_{aAH^{\bullet+}} = (2E^0_{AH/A^+,pH=0} - E^0_{AH/AH^{\bullet+}} + E^0_{A^\bullet/A^+})/0.058 \quad (1)$$

(all measurements were carried out at 20 °C).

Determination of the One-Electron Redox Potentials. In the absence of base, the reversible one-electron oxidation of MAHCN can be observed by means of cyclic voltammetry at ultramicroelectrodes at high potential scan rates v ($v >$ 13 000 V/s for Z = CN instead of $v >$ 1000 V/s for Z = H). $E^0_{AH/AH^{\bullet+}}$ is then obtained as the half-sum of anodic and cathodic peak potentials.

$MACN^+$ gives rise to a reversible one-electron cyclic voltammetric wave even at the lowest scan rate (0.1 V/s), whereas with MAH^+ a scan rate of at least 15 000 V/s is required to overcome the dimerization of the $MAH^\bullet$ radical, indicating that the dimerization of $MACN^\bullet$ is slow.[15] The corresponding standard potential is again obtained as the half-sum of anodic and cathodic peak potentials.

Determination of the Redox Potential for Hydride Transfer. A convenient method for obtaining the standard potential of hydride transfer for an unknown couple, $E^0_{A1H/A1^+}$, is to measure the rate constant of the following hydride transfer reaction

$$A1H + A2^+ \underset{k_{21}}{\overset{k_{12}}{\rightleftharpoons}} A1^+ + A2H$$

involving another NADH analogue couple for which $E^0{}_{AH/A+}$ is known.[16] Then

$$E^0_{A1H/A1^+} = E^0_{A2H/A2^+} - 0.029 \log K_{12} = E^0_{A2H/A2^+} - 0.029 \log(k_{12}/k_{21})$$

In practice, the time required for reaching the equilibrium is much too long to avoid the interference of side reactions. The only possibility is to derive K_{12} from the rate constants k_{12} and k_{21}. The equilibrium constant should not be too different from unity in order for both rate constants to be measurable. The very fact that $MACN^+$ is destabilized by the presence of the electron withdrawing cyano-group implies not only that D is large but also that MAHCN is a poor hydride donor. Among the NADH analogues whose E^0_{AH/A^+}'s are known in acetonitrile, the strongest hydride acceptor is *N*-benzyl-3-cyanoquinolinium, for which $E^0_{AH/A^+,pH=0} = 0.257 \pm 0.026$ V.[16b] Nonetheless, it is not a powerful enough hydride acceptor to abstract H^- from MAHCN at an appreciable rate in acetonitrile. We, therefore, had to use a more powerful hydride acceptor at low pH, namely 1,4-naphthoquinone (NQ),[14a] to obtain measurable rate constants. The overall reaction is

$$MAHCN + NQ + H^+ \underset{k_b}{\overset{k_f}{\rightleftharpoons}} MACN^+ + NQH_2$$

Thus

$$E^0_{MAHCN/MACN^+,pH=0} = E^0_{NQH_2/NQ,pH=0} - 0.029[pH + \log(k_f/k_b)]$$

In the CF_3CO_2H/CF_3COO^- buffer (pH 12.9[17]), both the forward and reverse reactions, starting with MAHCN + NQ and $MACN^+ + NQH_2$, respectively, proceed at appreciable rates. We thus found $k_f = 1.0 \pm 0.2$ M^{-1} h^{-1} and $k_b = 0.6 \pm 0.1$ M^{-1} h^{-1}. It follows that $E^0_{MAHCN/MACN^+,pH=0} = 0.370 \pm 0.028$ V[18] using for $E^0_{NQH_2/NQ,pH=0}$ a value of 0.750 ± 0.020 V.[15a] The main uncertainty in this determination comes from the electrochemical determination of $E^0_{NQH_2/NQ,pH=0}$ (0.02 over 0.028). The same is true for all the other NADH analogues, meaning that, relative one to the other, the standard potentials are known with a better precision than the absolute value of each of them.

Determination of the pK_a. Application of eq 1 then leads to $pK_{a\,MAHCN^{\bullet+}} = -4.4 \pm 1.1$. The main uncertainty again arises from the $E^0_{MAHCN/MACN^+,pH=0}$ through $E^0_{NQH_2/NQ,pH=0}$. This represents 0.7 unit over 1.1. As for the hydride transfer potential, the pK_a's are known, relative one to the other, with a better precision than the absolute value of each of them.

Homolytic Bond Dissociation Energy of the Cation Radical (*D*). The homolytic bond dissociation free energy may be obtained from the following thermochemical cycle

$$\Delta G^0_{AH^{\bullet+}/A^+ + H^\bullet} = E^0_{A^\bullet/A^+} + 0.058\ pK_{a,AH^{\bullet+}} - E^0_{H^\bullet/H^+}$$

In acetonitrile, $E^0_{H^\bullet/H^+} = -2.012$ V vs SCE.[19] Thus, $\Delta G^0_{MAHCN^{\bullet+}/MACN^+ + H^\bullet} = 1.77 \pm 0.07$ eV and the bond dissociation energy $D = \Delta G^0_{MAHCN^\bullet/MACN^+ + H^\bullet} + 0.348 = 2.115 \pm 0.066$ eV, assuming that the entropies of $MACN^+$ and $MAHCN^{\bullet+}$ are practically the same and taking the entropy of formation of $H^\bullet$ as 27.4 eu.[4a]

The last entry of Table 1 gives the values of the bond dissociation energy in the parent substrate, AH,

$$D_{AH/A^\bullet + H^\bullet} = E^0_{AH/AH^{\bullet+}} + D - E^0_{A^\bullet/A^+}$$

The weakening of the bond dissociation energy from the substrate, AH to the cation radical, $AH^{\bullet+}$ results from the aromatic character of A^+ as opposed to $A^\bullet$. The strengthening effect of the cyano substituent on the cation radical bond dissociation energy is the reflection of a stronger destabilization of the cation A^+ as compared to the cation radical itself. The fact that the cation radical energy is also affected by CN substitution is revealed by the positive shift of $E^0_{AH/AH^{\bullet+}}$ and the negative shift of the $pK_{a\,AH^{\bullet+}}$ (Table 1). This is confirmed by the substantial change that CN substitution induces in the UV−vis spectrum of the cation radical (Figure 1) as obtained from laser pulse experiments (see Experimental Section).

Kinetics of Cation Radical Deprotonation. The cyclic voltammograms of MAHCN at low scan rate obtained in the presence and in the absence of an excess of a base B, are shown in Figure 2. In the presence of a base, or in buffered medium BH^+/B, the anodic peak appearing in the first scan corresponds to a two-electron irreversible process. The reversible wave appearing in the second and third scans has the same characteristics as that of an authentic sample of $MACN^+$. It is

(15) It has already been reported that $MACN^\bullet$ exists in solution.[15b] (b) Happ, J. W.; Janzen, E. G.; Rudy, B. R. *J. Org. Chem.* **1970**, *35*, 3382.

(16) (a) Ostovic, D.; Lee, I.-S. H.; Roberts, R. M. G.; Kreevoy, M. M. *J. Org. Chem.* **1985**, *50*, 4206. (b) Anne, A.; Moiroux, J. *J. Org. Chem.* **1990**, *55*, 4608.

(17) (a) A spectrophotometric study of the CF_3CO_2H/pyridine equilibrium in acetonitrile gives $pK_{a\,CF_3CO_2H} = 12.9 \pm 0.1$, using a value of 12.3 for the pK_a of the pyridinium.[17b] The pK_a's of the pyridiniums in acetonitrile are from ref 17b. (b) Cauquis, G.; Deronzier, A.; Serve, D.; Vieil, E. *J. Electroanal. Chem.* **1975**, *60*, 205.

(18) It has been previously observed that there is a good parallelism between the values of $E^0_{MAHCN/MACN^+,pH=0}$ in acetonitrile and in 4/1 2-propanol/water, the values in acetonitrile being 0.290−0.340 V higher than in the aquoalcoholic mixture.[16a,b] MAHCN fits in the same correlation since the difference between the two solvents is 0.360 V.

(19) (a) Parker, V. D. *J. Am. Chem. Soc.* **1992**, *114*, 7458. (b) Parker, V. D. *J. Am. Chem. Soc.* **1993**, *115*, 1201 (erratum).

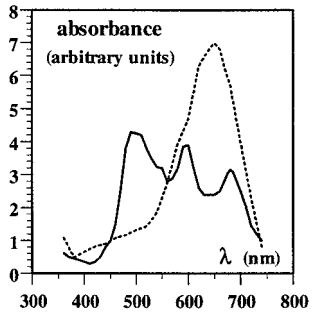

Figure 1. UV−vis absorption spectra of $MAHCN^{\bullet+}$ (full line) and $MAH_2^{\bullet+}$ (dashed line).

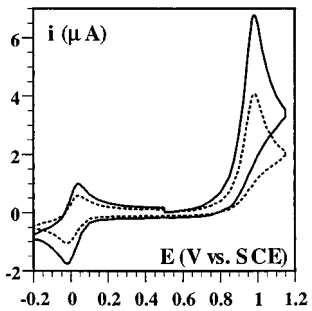

Figure 2. Cyclic voltammetry of MAHCN (1.01 mM) in acetonitrile + 0.1 M nBu_4BF_4 at 20 °C. Scan rate: 0.2 V/s platinum disk electrode (1 mm diameter). Dashed line: no base added. Continuous line: in the presence of 50 m*M* 2,4,6-trimethylpyridine. Potential scans: 0.5 ⇒ 1.15 V ⇒ −0.2 V ⇒ 0.5. Similar results were obtained at a glassy carbon disk electrode.

Scheme 3

$$P - e^- \rightleftharpoons Q$$

$$AH + Q \underset{k_{-e}}{\overset{k_{+e}}{\rightleftharpoons}} AH^{\bullet+} + P \quad [0]$$

$$AH^{\bullet+} + B \overset{k}{\rightleftharpoons} A^{\bullet} + BH^{+} \quad [1]$$

$$A^{\bullet} + Q \longrightarrow A^{+} + P \quad [2]$$

observed only when the first scan encompasses the irreversible oxidation wave. We may thus conclude that the two-electron oxidation of MAHCN in the presence of a base yields $MACN^+$ as with the other NADH analogues previously investigated.[14] The oxidation mechanism is thus as represented in Scheme 1, the second electron transfer step taking place, as shown before,[14] in solution (disproportionation) rather than at the electrode surface (ECE). Due to its huge driving force (0.975 eV, from the data in Table 1) the disproportionation reaction is under diffusion control, and the overall process is kinetically governed by the deprotonation step.

When no base is added, proton abstraction involves the substrate. Since the protonated substrate is not oxidized in the scanned potential range, the height of the whole voltammogram is divided by two as previously observed with the other NADH analogues.[14]

The deprotonation rate constant is too large to be conveniently measured by means of direct cyclic voltammetry. We thus resorted to homogeneous redox catalysis to measure this parameter. The principle of the method[20] is summarized in Scheme 3 (P/Q is the mediator reversible couple). As mediator, we selected benzoylferrocene. Its standard potential, $E^0_{P/Q}$ = 0.645 V, is close enough to the oxidation potential of the substrate for obtaining a significant catalytic increase of the peak height but not too close so that overlapping between the catalytic wave and the direct oxidation wave of the substrate is avoided. The driving force of reaction [2] is so large (0.645 V) that its rate constant is certainly close to the diffusion limit (10^{10} M^{-1} s^{-1}). Since $MAHCN^{\bullet+}$ is a strong acid, reaction [2] is much faster than the reverse reaction [1]. Forward reaction [1] may be regarded as irreversible. The ratio of the P oxidation peaks in the presence and in the absence of the substrate, i_p/i_p^0, is therefore a function of the kinetics of reactions [0] and [1]. The standard free energy of reverse of reaction [0] is $(RT/F)\ln(k_{+e}/k_{-e}) = -0.330$ eV. For the reaction between MAH_2 and the same mediator, benzoylferricenium, the standard free energy is −0.200 eV. k_{-e} was then found to be $10^{9.5}$ M^{-1} s^{-1}.[14c] The reaction between MAH_2 and ferricenium whose standard free energy is −0.450 V is diffusion-controlled.[14c] $10^{9.7}$ M^{-1} s^{-1} thus seems a reasonable estimate of k_{-e} in the present case. The value of k_{+e}, $10^{4.0}$ M^{-1} s^{-1}, ensues. Knowing k_{+e} and k_{-e}, the value of the rate constant k was derived, for each base, from the variations of i_p/i_p^0 with the concentrations of MAHCN, of P and B in Table 2 using already established working curves.[21] The data thus obtained are reported in Figure 3 under the form of a plot of log k vs the driving force of the deprotonation reaction expressed as $-\Delta G^0 = 0.058\ (pK_{a\,AH^{\bullet+}} - pK_{a\,BH^+})$. It clearly appears that in the explored driving force range, the deprotonation reaction is under activation control with a symmetry factor of *ca.* 0.3, similarly to what has been previously observed for the deprotonation of cation radicals of other NADH analogues.[14] The data points in Figure 3 may be fitted with a quadratic activation driving force equation ($\Delta G^{\ddagger}$ is the activation free energy and $\Delta G_0^{\ddagger}$ is the standard activation free energy

Table 2. Redox Catalysis Experiments for Determining the Deprotonation Rate Constants of the Cation Radical of MAHCN[a]

base	scan rate (V/s)	MAHCN conc.[b]	mediator conc.[b]	base conc.[b,c]
3-fluoropyridine	0.1, 0.2, 0.4	0.9	1.8	180−1600
pyridine	0.5, 1, 2	1.8	3.6	120−1200
		0.9	1.8	
3-methylpyridine	0.2, 0.4, 1, 2	1.8	3.6	2.5−72
		0.9	1.8	
3,5-lutidine	0.1, 0.2, 0.4	1	2	20−100
collidine	0.5, 1, 2	0.6	1.8	6−100

[a] The mediator was benzoylferrocene in all cases. [b] In mM. [c] Five to six concentrations in the indicated range.

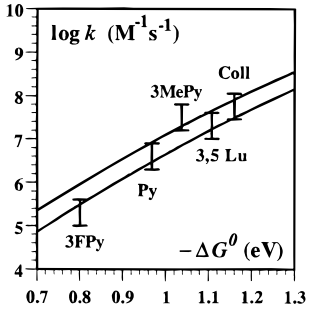

Figure 3. Variation of the deprotonation rate constant of $MAHCN^{\bullet+}$ with the driving force of the reaction (Lu: lutidine, Coll: collidine). The upper and lower lines correspond to $\Delta G_0^{\ddagger} = 0.69$ and 0.66 eV, respectively.

(20) Andrieux, C. P.; Savéant, J.-M. Electrochemical Reactions. In *Investigations of Rates and Mechanisms of Reactions*; Bernasconi, C. F., Ed.; Wiley: New York, 1986; Vol. 6, 4/E, Part 2, pp 305−390.

(21) (a) Andrieux, C. P.; Blocman, C.; Dumas-Bouchiat, J. M.; M'Halla, F. ; Savéant, J.-M. *J. Am. Chem. Soc.* **1980**, *102*, 3806. (b) Andrieux, C. P.; Savéant, J.-M. *J. Electroanal. Chem.* **1986**, *205*, 43. (c) Andrieux, C. P.; Anne, A.; Moiroux, J.; Savéant, J.-M. *J. Electroanal.* **1991**, *307*, 17.

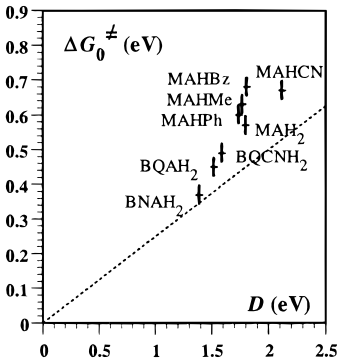

Figure 4. Correlation between the intrinsic barrier free energy and the homolytic bond dissociation energy. The dashed straight line represents $\Delta G_0^{\ddagger} = D/4$.

(intrinsic barrier):

$$k(\mathrm{M}^{-1}\,\mathrm{s}^{-1}) = 3 \times 10^{11} \exp\left(\frac{-F\Delta G^{\ddagger}}{RT}\right),$$

$$\Delta G^{\ddagger} = \Delta G_0^{\ddagger}\left(1 + \frac{\Delta G^0}{4\Delta G_0^{\ddagger}}\right)^2$$

The best fit is obtained for $\Delta G_0^{\ddagger} = 0.675 \pm 0.015$ eV.

Discussion

Figure 4 summarizes the correlation between the intrinsic barrier free energy, $\Delta G_0^{\ddagger}$, and the homolytic bond dissociation energy, D,[14] including the result for the cyano-derivative obtained as depicted in the preceding section. The error bars in Figure 4 have been estimated taking into account the fact that the same systematic error, due to the uncertainty on $E^0_{\mathrm{NQH_2/NQ,pH=0}}$, interferes both in $\Delta G_0^{\ddagger}$ and D. Putting aside, for the moment, the methylacridane derivatives bearing an alkyl or aryl group in the α position for which some sort of steric effect interferes (*vide infra*), it is seen that the α-cyanomethylacridane derivative, which has the largest bond dissociation energy, has also, as expected, the highest value of $\Delta G_0^{\ddagger}$. The correlation thus observed is close to proportionality between $\Delta G_0^{\ddagger}$ and $D/4$. We note, however, that the distance between the $D/4$ correlation and the data points increases as one passes from the BNA, to the BQN, BQCN, and MA ring. We propose the following model to explain these observations as well as the very fact that single Brönsted plots are obtained when anyone of the NADH analogue cation radicals is opposed to a series of normal nitrogen or oxygen bases.

We consider successively three types of reactions: the self-exchange reaction between a normal acid and its conjugate base (for example pyridine); the self-exchange reaction between a NADH analogue cation radical, $AH^{\bullet+}$, and its conjugate base, *viz.*, the radical $A^{\bullet}$; and the reaction of a NADH analogue cation radical, $AH^{\bullet+}$, with a normal base such as pyridine (Scheme 4). In all cases, the reaction starts with the formation of a precursor complex and ends with the dissociation of a successor complex (Scheme 4). In the gas phase, the homolytic and ionic dissociation profiles of PyH^+ are of the type shown in Figure 5a. Dissociation of PyH^+ into Py and H^+ requires a much larger energy, 9.22 eV, than the homolytic dissociation ($PyH^+ \leftrightarrow Py^{\bullet+} + H^{\bullet}$), 4.90 eV.[22] The covalent profile is a Morse curve

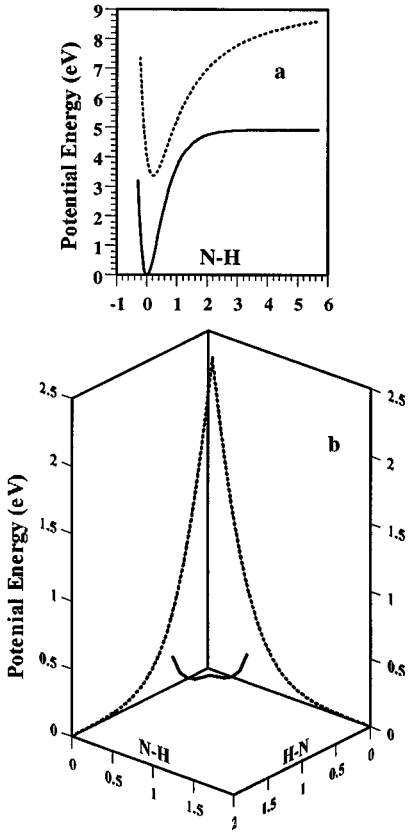

Figure 5. (a) Homolytic (full line) and ionic (dashed line) dissociation of the pyridinium ion. (b) Homolytic hypothetical reaction pathways (dashed line) and actual ionic reaction pathway (full line). Distances are in Å.

$$G_{\mathrm{cov}} = D\{1 - \exp[-\beta(x - x_0)]\}^2$$

where x the N−H distance, $x_0 = 1.033$ Å is the equilibrium distance, $D = 4.90$ eV, β (Å^{-1}) $= 1.357\ 10^{-3}\ \upsilon$ (cm^{-1}), and (D (eV))$^{-1/2} = 2.02$.[23] The ionic profile

$$G_{\mathrm{ionic}} = \Delta G_I + D\{\exp[-\beta(x - x_0)]\}^2 - C\left(\frac{1}{x} - \frac{1}{x + a}\right)$$

(ΔG_I is the heterolytic bond dissociation free energy) was grossly estimated assuming that, due to the polarizability of the pyridine molecule, there is a unit positive charge on the hydrogen and on the para-carbon and a unit negative charge on the nitrogen ($a = 2.72$ Å) with a repulsive term equal to the Morse repulsive term. $C = 14.4$ eV × Å. It thus appears that the dissociation of an isolated PyH^+ molecule in the gas phase should preferably undergo a homolytic rather than an ionic dissociation.

However, in spite of a possibly modest contribution of the ionic state, as compared to the covalent state in the ground state of PyH^+, its dissociation triggered by the approach of a pyridine molecule is far from following a homolytic pathway such as the one represented by the dashed line in Figure 5b.[24] The approach of the pyridine molecule immediately enhances the contribution of the ionic state so as to result in the classical double well profile with a very small activation barrier, if any. Recent *ab initio* calculations on water and ammonia, taking into account electron correlation at the MP2 level, indeed show that

(22) (a) Combining the data from refs 22b and 4a. (b) Aue, D. H.; Bowers, M. T. *Stabilities of positive ions from equilibrium gas-phase basicity measurements in Gas Phase Ion Chemistry*; Bowers, M. T., Ed.; Academic Press: New York, 1969; Vol. 2, Chapter 9, p 1.

(23) (a) $\upsilon = 3300$ cm^{-1}.[23b] $x_0 = 1.033$ Å.[23c] (b) Socrates, G. *Infrared Characteristic Group Frequencies*; Wiley: New York, 1994; p 132. (c) *Handbook of Chemistry and Physics*, 72nd ed.; CRC Press: 1991−92; pp 9−11.

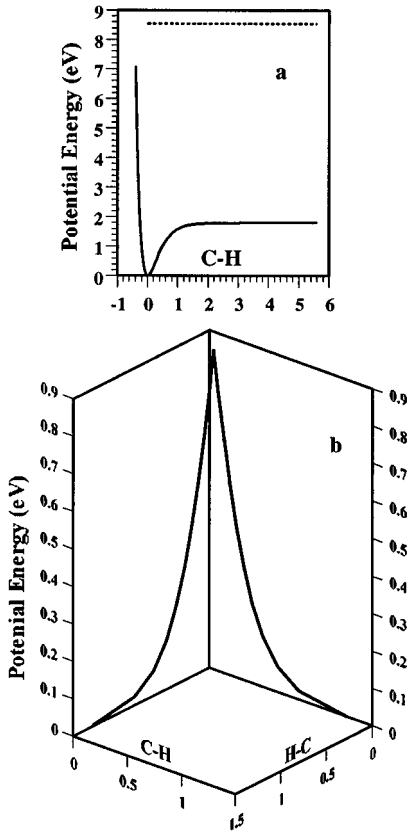

Figure 6. (a) Homolytic (full line) and ionic (dashed line) dissociation of $AH^{\bullet+}$. (b) Homolytic hypothetical reaction pathways in the $AH^{\bullet+}$+ $A^{\bullet}$ self-exchange reaction. Distances are in Å.

there is practically no barrier in the gas phase and a very small barrier the liquid phase.[26] The results of these calculations are reproduced in Figure 5b, neglecting the small changes that may occur when passing from water or ammonia to pyridine, in order to provide a rough idea of the huge energy difference favoring the ionic pathway over the homolytic pathway.

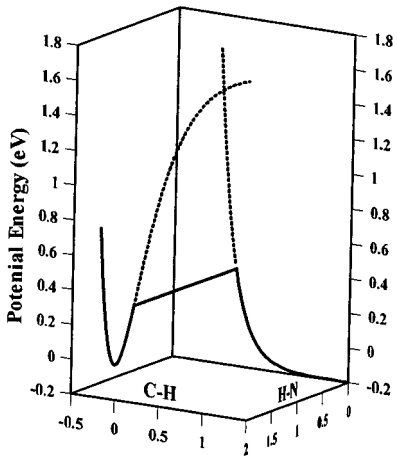

Figure 7. Reaction pathway in the reaction $AH^{\bullet+} + B \rightarrow A^{\bullet} + BH^{+}$. Distances are in Å.

What happens with the $AH^{\bullet+} + A^{\bullet}$ self-exchange reaction is illustrated in Figure 6 with the example of methylacridane cation radical. In the gas phase, the homolytic dissociation is much easier than the ionic dissociation (1.8 eV vs 8.55 eV[27]). The approach of H^{+} to $A^{\bullet}$ is not likely to result in a strong stabilization, leading to the notion that the contribution of the ionic state to the ground state at equilibrium distance should be small, much smaller than in the case of PyH^{+} (Figure 6a). Likewise, in the self-exchange reaction, the presence of $A^{\bullet}$ in the vicinity of $AH^{\bullet+}$ within the encounter complex (Scheme 4) is not expected to induce a significant stabilization of the ionic state, $A^{\bullet}\ H^{+}\ {}^{\bullet}A$. It thus appears that the homolytic pathway represented in Figure 6b[24] should be energetically preferred.

Figure 7 represents what should be the preferred pathway for the reaction of $AH^{\bullet+}$ with a normal base such as pyridine. Within the precursor complex (Scheme 4), the presence of the base does not induce any particular change in the homolytic state describing the cation radical $AH^{\bullet+}$ ($A^{+}\ {}^{\bullet}H$) when the C−H elongates. In contrast, the ionic state of the cation radical ($A^{\bullet}\ {}^{+}H$) is strongly stabilized by the presence of the base as the C−H distance increases. Taking into account the absence of significant barrier in the PyH^{+} + Py reaction, we may thus infer that the potential energy curve of the products in the successor complex simply contains a repulsive term resulting from the decrease of the distance between the H and C atoms and the concomitant bending of the C−R bond. The main effect of the base is thus to poise the height of the repulsive curve at a value corresponding to the standard free energy change between the precursor and successor complexes, $\Delta G^{0\prime}$. The repulsive curve in the successor complex may be approximated by the repulsive part of the Morse curve of the reactant system by analogy with the dissociative electron transfer theory.[25] The reaction path (Figure 7 where the characteristic parameters are those of $MAH_2^{\bullet+}$ and $\Delta G^{0\prime} = -0.2$ eV) and the free energy of activation may therefore be derived from the following equations.

$$G^{0}_{\text{reactants, precursor}} = D\{1 - \exp[-\beta(x - x_0)]\}^2$$

$$G^{0}_{\text{products, successor}} = \Delta G^{0\prime} + D\{\exp[-\beta(x - x_0)]\}^2$$

It follows[25] that the free energy for $\Delta G^{0\prime} = 0$ is one-fourth of the bond dissociation energy.

(24) (a) The homolytic reaction profile is obtained by intersection of the two following surfaces and determination of the saddle point on the intersection[24b]

$$G_{\text{reactants}} = D\{1 - \exp[-\beta(x - x_0)]\}^2 + D\{\exp[-\beta(y - y_0)]\}^2$$

$$G_{\text{products}} = D\{\exp[-\beta(x - x_0)]\}^2 + D\{1 - \exp[-\beta(y - y_0)]\}^2$$

(x and y are the first and second N−H or C−H distances, respectively, and x_0 and y_0 are their equilibrium values). It follows that the reaction pathway is defined by the following equations

$$\exp[-\beta(x - x_0)] + \exp[-\beta(y - y_0)] = 1$$

$$x_0 \le x \le x_0 + (1/\beta)\ln 2 \quad G = 2D\{\exp[-\beta(x - x_0)]\}^2$$

$$(y_0 + (1/\beta)\ln 2 \le y \le \infty)$$

$$y_0 \le y \le y_0 + (1/\beta)\ln 2 \quad G = 2D\{\exp[-\beta(y - y_0)]\}^2$$

$$(x_0 + (1/\beta)\ln 2 \le x \le \infty)$$

The activation barrier is thus equal to $D/2$.[24d] (b) Similarly to a model recently developed for S_N2 substitution[24c] based itself on an earlier model of dissociative electron transfer.[25] (c) Marcus, R. A. *J. Phys. Chem. A* **1997**, *101*, 4072. (d) In reality, owing to avoided crossing at the saddle point the reaction path goes through a rounded maximum, somewhat lower than the sharp discontinuous maximum shown in Figures 5b and 6b.

(25) (a) Savéant, J.-M. *J. Am. Chem. Soc.* **1987**, *109*, 6788. (b) Savéant, J.-M. *Acc. Chem. Res.* **1993**, *26*, 455. (c) Savéant, J.-M. *J. Am. Chem. Soc.* **1992**, *114*, 10595. (d) Savéant, J.-M. Dissociative Electron Transfer in *Advances in Electron Transfer Chemistry;* Mariano, P. S., Ed.; JAI Press: New York, 1994; Vol. 4, pp 53−116.

(26) (a) Tuñón, I. ; Tortonda, F. R.; Pascual-Ahuir, J. L.; Silla, E. *J. Mol. Struct. (Theochem)* **1996**, *371*, 117. (b) Tortonda, F. R.; Pascual-Ahuir, J. L.; Silla, E.; Tuñón, I. *J. Phys. Chem.* **1995**, *99*, 12525. (c) Tortonda, F. R.; Pascual-Ahuir, J. L.; Silla, E.; Tuñón, I. *J. Phys. Chem.* **1993**, *97*, 11087.

Scheme 4

Pyridinium + Pyridine Self Exchange

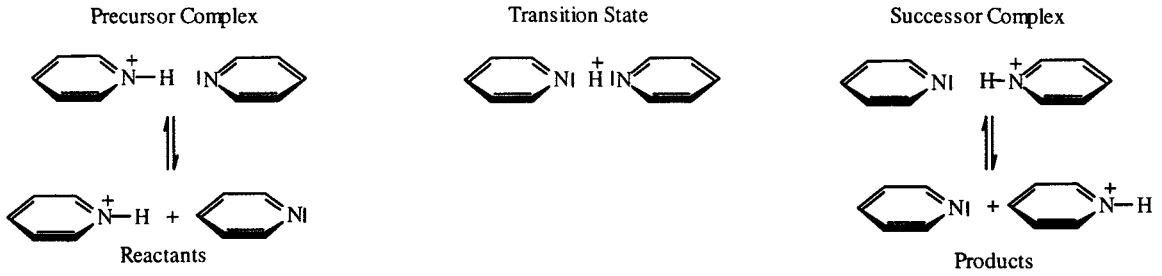

NADH Cation Radical + NAD Radical Self Exchange

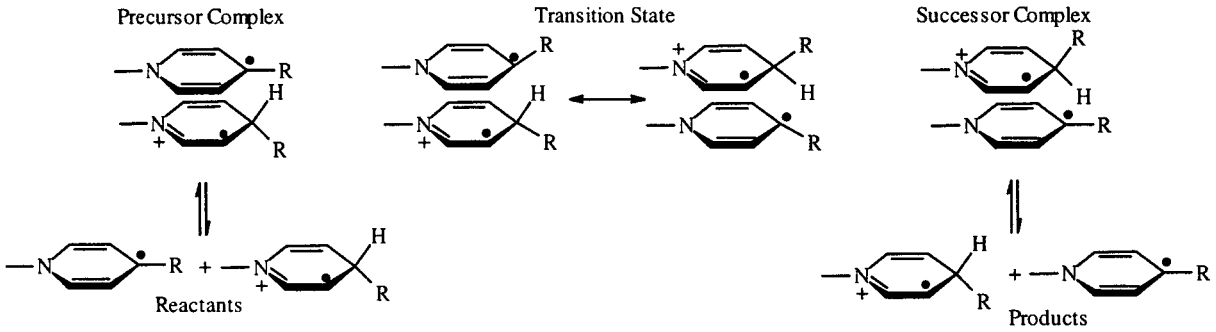

NADH Cation Radical + Pyridine

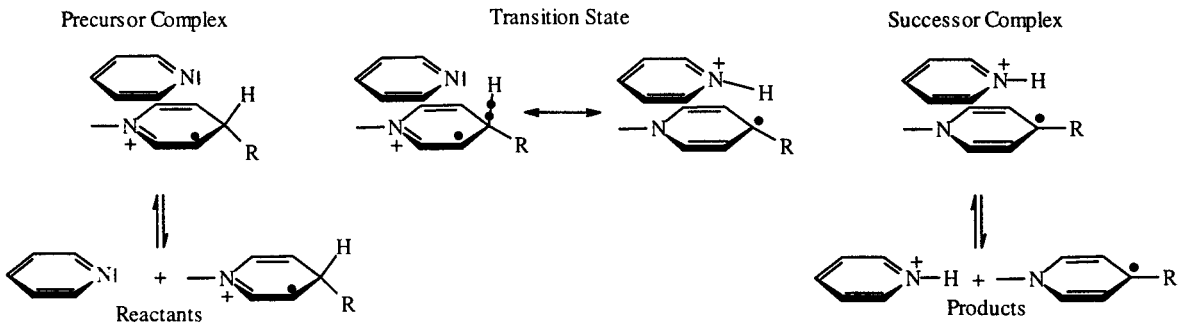

$$\Delta G^{\ddagger}_{\Delta G^{0\prime}=0} = D/4$$

In addition to bond breaking, solvent reorganization is expected to contribute to the barrier.

$$\Delta G^{\ddagger}_{\Delta G^{0\prime}=0} = (D/4) + (\lambda_0/4)$$

This factor is however likely to be small (of the order of 0.1 eV in view of the dimensions of the species involved[28]) since the charge in the precursor and successor complexes are spread over a rather large volume. $\Delta G^{\ddagger}_{\Delta G0'=0}$ is related to the intrinsic barrier, $\Delta G^{\ddagger}_0 = \Delta G^{\ddagger}_{\Delta G0'=0}$, that we have derived from the rate data as follows. The total standard free energy of the reaction, from separated reactants to separated products, ΔG^0, is related to the standard free energy change from the precursor to the successor complexes, $\Delta G^{0\prime}$, according to

$$\Delta G^{0\prime} = \Delta G^0 + w_R + w_P$$

where w_R and w_P are the reactant and product work terms, i.e., the standard free energy difference between the precursor complex and the separated reactants, on the one hand, and between the successor complex and the separated products, on the other.[25] The following equations ensue:

$$\Delta G^{\ddagger} = w_R + \Delta G^{\ddagger}_{\Delta G^{0\prime}=0}\left(1 + \frac{\Delta G^{0\prime}}{4\Delta G^{\ddagger}_{\Delta G^{0\prime}=0}}\right)^2$$

$$\Delta G^{\ddagger}_{\Delta G^{0}=0} = w_R + \Delta G^{\ddagger}_{\Delta G^{0\prime}=0}\left(1 + \frac{w_P - w_R}{4\Delta G^{\ddagger}_{\Delta G^{0\prime}=0}}\right)^2 \approx$$

$$\Delta G^{\ddagger}_{\Delta G^{0\prime}=0} + \frac{w_R + w_P}{2} \approx \frac{D}{4} + \frac{w_R + w_P}{2} + \frac{\lambda_0}{4}$$

The model thus provides an explanation of two important features of the experimental results, namely, (i) a given cation radical gives rise to a single Brönsted plot when opposed to a series of normal bases and (ii) the correlation between the

(27) See footnote d in Table 5 of ref 14c. $\beta = 2.8$ Å^{-1} was obtained from[25d] $\beta_{AH^{\bullet+}} = (D_{AH}/D_{AH^{\bullet+}})^{1/2}$, taking for ν, the frequency found for acridane, 2900 cm^{-1}.

(28) (a) Marcus, R. A. *J. Chem. Phys.* **1956**, *24*, 966. (b) Marcus, R. A. *J. Chem. Phys.* **1956**, *24*, 979. (c) Hush, N. S. *J. Chem. Phys.* **1958**, *28*, 962. (d) Hush, N. S. *Trans. Faraday Soc.* **1961**, *57*, 557. (e) Marcus, R. A. *J. Chem. Phys.* **1965**, *43*, 679.

Table 3. Thermodynamics and Kinetics of the Deprotonation of $(p\text{-An})_2NCH_2H^{\bullet+}$ by Quinuclidines[a]

$pK_{a\,BH^+} - pK_{a\,AH^{\bullet+}}$	ΔG^0 (eV)	log k ($M^{-1}\,s^{-1}$)	$\Delta G^{\ddagger}$ [b] (eV)	$\Delta G_0^{\ddagger}$ [c] (eV)
9.5	−0.54	4.8	0.35	0.59
8.7	−0.50	4.35	0.38	0.60
6.55	−0.37	2	0.46	0.63
5.4	−0.31	2.2	0.50	0.65
				av 0.62

[a] In acetonitrile at 15 °C. [b] $\Delta G^{\ddagger} = 0.05718\ (11 - \log k)$. [c] From $\Delta G^{\ddagger} = \Delta G_0^{\ddagger}(1 + \Delta G^0/4\Delta G_0^{\ddagger})^2$.

intrinsic barrier and the bond dissociation energy is close to a proportionality of $D/4$.

The most significant deviation from this proportionality occurs in the methylacridane series when one of the hydrogens is replaced by an aryl or an alkyl group (Figure 4). $\Delta G_0^{\ddagger}$ then increases in the order H < Ph < Me < Bz, while the bond dissociation energy remains about the same. From the representation of the precursor and successor complexes given in Scheme 4, we see that the steric hindrance resulting from the presence of the aryl or an alkyl groups tends to increase w_P, while w_R is not affected. An increase of $\Delta G_0^{\ddagger}$ ensues. It is minimal with MAHPh since the rotation of the phenyl group around the C−C bond is hindered by its conjugation with the MA ring in the $MAHPh^{\bullet}$ radical. It then increases, as expected from Me to Bz.

We also note that, in the AH series, the deviation from the proportionality to $D/4$ increases with the number of rings in the A moiety. This observation can be explained by a variation of the reactant work term, w_R. With one ring, as with $BNAH_2$, the interaction between the base and the cation radical is relatively strong. It decreases when passing to $BQAH_2$ (and $BQCNH_2$) and to MAH_2, owing to the increase delocalization of the positive charge over a larger and larger molecular framework.

There are a few *other cation radicals* for which Brönsted plots with opposing normal bases are available. One series involves the cation radicals of polymethylbenzenes (hexamethyl, pentamethyl, 1,2,4,5- and 1,2,3,4-tetramethyl).[6b] As noted earlier,[14c] the intrinsic barriers are very close to $D/4$ (the intrinsic barrier is practically the same for all four cation radicals and equal to 0.6 eV, the bond dissociation energy is also the same, and $D/4 = 0.59$ eV). Another interesting example is the deprotonation of $(p\text{-An})_2NCH_2H^{\bullet+}$ (An: anisyl) by a series of diversely substituted quinuclidines.[8a] The results are summarized in Table 3. Here again the intrinsic barrier, 0.62 eV, is remarkably close to $D/4$ (0.51 eV).

Experimental Section

Chemicals. All chemicals, including 9-cyano-10-methylacridinium methyl sulfate $MACN^+$, $CH_3SO_3^-$, were from Aldrich Chemical Co. Commercial products were of the highest purity available and were used as received. 9-Cyano-10-methylacridan (MAHCN) was prepared by adaptation of a previously described procedure.[15b] 10-Methylacridinium iodide MAH^+, I^- (1.3 g), prepared as in ref 29, was dissolved in 50 mL of a DMSO/water mixture (90/10). KCN (0.15 g) was then added, and the reaction was allowed to proceed in the dark, at room temperature under a nitrogen atmosphere, for 5 h. Addition of 50 mL of water brought about the precipitation of MAHCN which was filtered, washed with $CHCl_3$, and crystallized from methanol/water. Final yield: 60%.

Instrumentation and Procedures. The instrumentation and procedures were the same as previously described[14] except for the determination of the standard redox potential of hydride transfer of the MAHCN/$MACN^+$ couple. In 50 mM CF_3COOH + 25 mM Me_4NOH buffered acetonitrile, $MACN^+$ exhibits a maximum of absorption at 384 nm with a molar absorbance of 20 000 $M^{-1}\,cm^{-1}$. MAHCN as well as NQ and NQH_2 do not absorb appreciably at this wavelength. Therefore starting either with MAHCN (2 mM) + NQ (20 mM) or $MACN^+$ (1 mM) + NQH_2 (10 mM), the MA^+CN concentration can be monitored through the measurement of the absorbance at 384 nm. Pseudo-first-order kinetics were observed for the production or the consumption of $MACN^+$ over periods of 24 h or more.

Conclusions

The 9-cyano substituted methylacridane gives rise to a cation radical that has the highest value of the homolytic bond dissociation energy in the NADH analogue family owing to the strong destabilization of the cation by the cyano group. Deprotonation by normal bases gives rise to an activation controlled single Brönsted plot as for the other cation radicals of the same family. Over the whole series, the intrinsic barrier correlates with the homolytic bond dissociation energy. In the absence of significant steric hindrance, the correlation is close to proportionality of the intrinsic barrier to one-fourth of the dissociation homolytic bond dissociation energy. The same result is found for other cation radicals for which previous studies have shown that their deprotonation by normal bases gives rise also to single Brönsted plots (polymethylbenzenes, *p*-dianisylmethylamine).

The respective contributions of the homolytic and ionic states in the dissociation of the two types of acids, cation radical and the conjugate acid of the normal base, are such that a simple model can be developed which regards the deprotonation reaction as a concerted H atom/one-electron transfer. The model predicts, in agreement with experiment, (i) that, for each radical cation, the deprotonation kinetics follows an activation controlled single Brönsted plot and (ii) that the major part of the intrinsic barrier is related to the homolytic dissociation of the C−H bond of the cation radical entailing a contribution equal to one-fourth of the bond dissociation energy.

Deviations from this behavior due to the presence of bulky substituents on the functional carbon can be explained by the introduction of a product work term in the model expressing the difference in free energy between the successor complex and the separated products. Minor deviations from the $D/4$ proportionality depending on the extent of charge delocalization over the cation radical molecule may be accounted for by a reactant work term expressing the difference in free energy between the precursor complex and the separated reactants.

JA973725K

(29) Roberts, R. M. G.; Ostovic, D.; Kreevoy, M. M. *Faraday Discuss. Chem. Soc.* **1982**, *74*, 257.